



**HAL**  
open science

## Cadmium(II) recovery from hydrochloric acid solutions using Amberlite XAD-7 impregnated with a tetraalkyl phosphonium ionic liquid

R. Navarro, V. Gallardo, M. Martinez, E. Guibal, A. Arias, I. Saucedo

► **To cite this version:**

R. Navarro, V. Gallardo, M. Martinez, E. Guibal, A. Arias, et al.. Cadmium(II) recovery from hydrochloric acid solutions using Amberlite XAD-7 impregnated with a tetraalkyl phosphonium ionic liquid. *Reactive and Functional Polymers*, 2011, 71 (11), pp.1059-1070. 10.1016/j.reactfunctpolym.2011.07.008 . hal-02949483

**HAL Id: hal-02949483**

**<https://hal.science/hal-02949483>**

Submitted on 26 Jun 2024

**HAL** is a multi-disciplinary open access archive for the deposit and dissemination of scientific research documents, whether they are published or not. The documents may come from teaching and research institutions in France or abroad, or from public or private research centers.

L'archive ouverte pluridisciplinaire **HAL**, est destinée au dépôt et à la diffusion de documents scientifiques de niveau recherche, publiés ou non, émanant des établissements d'enseignement et de recherche français ou étrangers, des laboratoires publics ou privés.

# Cadmium(II) recovery from hydrochloric acid solutions using Amberlite XAD-7 impregnated with a tetraalkyl phosphonium ionic liquid

A. Arias<sup>a</sup>, I. Saucedo<sup>a</sup>, R. Navarro<sup>a,\*</sup>, V. Gallardo<sup>a</sup>, M. Martinez<sup>a</sup>, E. Guibal<sup>b</sup>

<sup>a</sup> Universidad de Guanajuato, División de Ciencias Naturales y Exactas, Departamento de Química, Cerro de la Venada s/n, Pueblito de Rocha, C.P. 36040 Guanajuato, Gto, Mexico

<sup>b</sup> Ecole des Mines Alès, Laboratoire Génie de l'Environnement Industriel, Equipe Interfaces Fonctionnalisées pour l'Environnement et la Sécurité, 6, avenue de Clavières, F-30319 Alès cedex, France

## ABSTRACT

Cyphos<sup>®</sup> IL-101 (tetraalkyl phosphonium ionic liquid, IL) was immobilized in a synthetic resin (Amberlite XAD-7) for preparing an solvent impregnated resin (SIR). This SIR was tested for Cd(II) sorption in HCl solutions. Optimum sorption occurs for HCl concentrations close to 3–4 M through an ion exchange mechanism involving phosphonium cation and  $\text{CdCl}_4^{2-}$ . Sorption capacity increased with IL loading, though a fraction of the IL remained inactive, being bound to the polymer support. Sorption capacity is poorly influenced by metal ions that do not form chloroanionic species. Uptake kinetics are controlled by the resistance to intraparticle diffusion. The intraparticle diffusivity coefficient increased with temperature, initial metal concentration but decreased with increasing IL loading (probably due to a decrease of the interfacial area and a slow diffusion of metal ions in the organic phase that fills the porous network). Metal desorption and resin recycling can be performed using nitric acid (0.1 M) with sorption and desorption performances maintained for at least five cycles.

### Keywords:

Phosphonium ionic liquid  
Cyphos IL 101  
Amberlite XAD-7  
Cadmium recovery  
Solvent impregnated resin

## 1. Introduction

The regulations concerning metal discharge to the environment are becoming more and more drastic. Uncontrolled release to the environment may cause serious health problems due to their accumulating effect in the food chain. For example, the case of mercury contamination in the Minamata bay in Japan showed that the accumulation of the metal along the food chain induced dramatic damages. Cadmium is also part of the topic contaminants that retained great attention from Health Authorities and Regulation Agencies. Indeed, cadmium intake may have long-term effects such as kidney damage, or impact on blood, bone and liver. Short-term exposure may cause diarrhea, vomiting, nausea.

Apart of environmental impacts, the ethical and political demand for sustainable growth requires from industry developing processes for minimizing waste production and in a growing number of countries the final discharge to landfill is only authorized after proving that the material cannot be valorized. For this reason there is a need for the recovery of metals from secondary sources (including low-grade ores and industrial wastes). Cadmium is widely used in Ni–Cd batteries. Hydrometallurgy can be used to recover and separate these metals: the first step (after dismantling the material and magnetic separation) consists in bioleaching or

acidic leaching using sulfuric acid or hydrochloric acid [1–3]. Several methods can be used for cadmium binding: sorption using different materials such as ion exchange resins [4–6], biosorbents [7,8], activated carbon [9], polymer inclusion membranes [10], solvent extraction [2,11], extractant impregnated resins [12–24].

Polymers-supported reagents are widely employed in metal ions separations [25,26]. Extractant impregnated resins have retained much attention for the last decades. Indeed, immobilizing an extractant in a resin support allows maintaining their high recovery efficiency and preventing their dispersion in the aqueous solution (expensive and hazardous compounds). Additionally, the presence of the resin may enhance the removal efficiency of the extractant. For example, Muraviev et al. [27] compared the extraction behavior of DEHPA and DEHDTPA toward Cu(II)/Zn(II) mixtures in the bi- and triphase systems of different types. They showed that the presence of the resin significantly facilitates the solvent extraction of the ionic species that are not extracted in the liquid/liquid systems; they attributed this effect to the changes of both hydration of metal ions and pH in the resin phase [27].

Different methods of SIR preparation have been published [28]. More recently, new SIR have been designed [29]. Different strategies have been proposed using biopolymers for the immobilization of the extractant [30,31], using less hazardous extractants (ionic liquids) immobilized in conventional resins [32,33], or in biopolymer matrices [34–39]. Ionic liquids offer very promising properties for metal recovery in solvent extraction processes; among them, Cyphos products (based on the chemistry of tetraalkyl

\* Corresponding author. Tel./fax: +52 473 732 7555.

E-mail address: navarm@ugto.mx (R. Navarro).

phosphonium salts) have been tested for the recovery of Pd(II) and Zn(II) [40–42]. Metals forming anionic complexes with chloride ions can be bound in 1–5 M HCl solutions [32–42]. They have been also used for the extraction of organic compounds [43–45].

This work focuses on the synthesis of a SIR based on the immobilization of Cyphos® IL-101 (tetraalkyl phosphonium chloride) in Amberlite XAD-7 and its application to recovery of Cd(II) from HCl solutions. The SIR are characterized using optical microscopy, scanning electron microscopy coupled with energy dispersive X-ray microanalysis (SEM-EDAX), and textural analysis, looking at the impact of IL loading. The sorption properties are studied evaluating the impact of HCl concentration, the sorption isotherms, and the effect of the presence of competitor ions. The kinetics are investigated with the double objective of identifying the limiting step in the mass transfer and measuring the effect of increasing the IL loading on the resistance to intraparticle diffusion. The last part deals with metal desorption and SIR recycling. A great attention is paid to the understanding of IL loading on sorption capacity (availability of IL) and uptake kinetics (mass transfer properties).

## 2. Materials and methods

### 2.1. Materials

Amberlite XAD-7 was supplied by Sigma–Aldrich (Saint-Louis, USA). This is a polyacrylic acid ester type resin ( $[\text{CH}_2\text{-CH}(\text{COOR})]_n$ ). The physical characteristics of the resin are summarized in Table 1 [32]. Amberlite XAD-7 can be considered as a nonionic, moderately hydrophilic porous polymer (pore diameter: 90 Å). It is commercialized as a macroporous polymer, although it must be considered as a mesoporous material (pore diameter: 20–500 Å) according to IUPAC. The resin was conditioned by the supplier with NaCl and  $\text{Na}_2\text{CO}_3$  to retard bacterial growth. It was necessary to clean it to remove salts and monomeric material present on the resin. The resin was therefore put into contact with ketone for 24 h at 25 °C. After filtration under vacuum to remove excess ketone, the resin was rinsed with de-mineralized water. Then, it was washed with nitric acid (0.1 M) for 24 h. The resin was filtered under vacuum and then rinsed with de-mineralized water to constant pH. Finally, the resin was put into contact with ketone for 12 h before being filtered under vacuum and dried in a roto-vapor at 80 °C. Cyphos® IL-101 was kindly supplied by Cytec (Canada). This is a phosphonium salt (tetradecyl(trihexyl)phosphonium chloride, C.A.S. number: 258864-54-9, formula weight: 519.4 g mol<sup>-1</sup>). It is a slightly viscous room temperature ionic liquid. It is less dense than water and colorless to pale yellow. It is immiscible with water although it is sparingly soluble in water and can dissolve up to 8% water. The chemical structure is  $[\text{P R}_3\text{R}'^+] \text{Cl}^-$ , where R = hexyl and R' = tetradecyl. Other reagents (salts, acids, etc.) were analytical grade and supplied by KEM (Mexico). Standard metal solutions were supplied by Perkin Elmer (USA).

### 2.2. Resin impregnation

In the present work the extractant was immobilized on the resin by a physical technique. Different processes may be used

**Table 1**  
Physical characteristics of Amberlite XAD-7 resin [32].

Parameter	Value
Particle size	20/60 mesh – 250–850 μm
Specific surface area	450 m <sup>2</sup> g <sup>-1</sup>
Resin porosity	0.55
Pore size (mean value)	85–80 Å
Pore volume	0.97–1.14 cm <sup>3</sup> g <sup>-1</sup>
Skeletal density	1.24 g cm <sup>-3</sup>

for the physical impregnation of the resin including (i) the wet method, (ii) the dry method, (iii) the impregnation in the presence of a modifying agent, or (iv) the dynamic method [46]. Previous studies have shown that the dry method increases the stability of the extractant on the resin. The dry impregnation of the resin was actually performed by contact of 5 g of conditioned Amberlite XAD-7 with 25 mL of ketone for 24 h. Varying amounts of Cyphos® IL-101 diluted in ketone (0.5 M) were added to resin slurry for 24 h, under agitation. The solvent was then slowly removed by evaporation in a roto-vapor. The amount of extractant immobilized on the resin ( $q_{\text{Cyphos IL-101}}$ ) was quantified by the following procedure. A known amount of impregnated resin (250 mg) was mixed with methanol (5 mL) for 24 h to dissolve the extractant and the solvent was separated from the resin by decantation. This washing treatment was carried out twice. Finally, the resin was dried at 50 °C for 24 h for complete evaporation of solvent. The mass difference ( $M_{\text{Cyphos IL-101}}$ ) between impregnated ( $M_{\text{XAD-7/Cyphos IL-101}}$ ) and washed resin ( $M_{\text{XAD-7}}$ ) was used to calculate the amount of extractant immobilized on the SIR:

$$q_{\text{Cyphos IL-101}} = \frac{M_{\text{XAD-7/Cyphos IL-101}} - M_{\text{XAD-7}}}{M_{\text{XAD-7/Cyphos IL-101}}} \quad (1)$$

The experimental procedure allowed the preparation of SIR containing 25 mg extractant g<sup>-1</sup> up to 595 mg extractant g<sup>-1</sup>. Table 2 reports the characteristics of a series of impregnated resins prepared according this procedure and for the evaluation of impregnation method, optical microscopy, and textural analysis. For sorption experiments another series of impregnated resins were used with the following IL contents: 48, 99, 144, 200, 287, 416, 493 and 595 mg IL g<sup>-1</sup> SIR.

### 2.3. Characterization

For the textural characterization of SIR, nitrogen N<sub>2</sub> adsorption isotherms were obtained using a BET surface area analyzer (Micromeritics ASAP 2010). The adsorption isotherms were used for the determination of the specific surface area, the pore size and the pore volume, following the BET method [47], and the Kelvin equation [48]. The resins were initially conditioned under vacuum at 50 °C (to remove the gas contained in the porous network, and measure the dry weight of the sample) before varying the pressure of gas (i.e., N<sub>2</sub>) in the tank, and measuring at equilibrium the volume of gas adsorbed and the saturation pressure.

The macroscopic characteristics (external aspect) of the SIR were obtained from an optical digital stereomicroscope (National DCS-420TH). Element distribution (especially Cd and P, as the tracers of metal sorption and IL distribution, respectively) in the beads was investigated by Environmental Scanning Electron Microscopy (ESEM) Quanta FEG 200, equipped with an OXFORD Inca 350 energy dispersive x-ray microanalysis (EDAX) system. The system can be used to acquire qualitative or quantitative spot analyses and qualitative or quantitative X-ray elemental maps and line scans. This ESEM allows analyzing samples at pressures and humidity levels that approach normal laboratory conditions and avoids experimental artifact. The preparation of the cross-section of impregnated resin was performed by particle freezing in liquid nitrogen followed by knife cutting of the spherical particles.

### 2.4. Sorption and desorption studies

Cd(II) solutions were prepared in HCl solutions of different concentrations (0.001–8 M) with metal concentrations ranging between 5 and 200 mg Cd L<sup>-1</sup>. The sorption experiments were performed by mixing the resin with Cd(II) solutions for 24 h with a solid/liquid ratio (sorbent dosage, SD) fixed to  $m/V = 4 \text{ g L}^{-1}$

**Table 2**

IL loading for different lots of Cyphos IL-101 impregnated Amberlite XAD-7 resins (for surface analysis and optical microphotographs).

Resin	L1	L2	L3	L4	L5	L6	L7	L8	L9	L10
IL loading (mg g <sup>-1</sup> )	25	50	88	101	139	193	310	402	487	579
IL loading (mmol g <sup>-1</sup> )	0.048	0.096	0.169	0.195	0.277	0.372	0.597	0.774	0.938	1.115

( $m$ : mass of sorbent,  $V$ : volume of solution). The contact was operated on a reciprocal shaker (Cole Parmer 51502) with an agitation speed of 150 movements per minute at constant temperature. After filtration the samples were analyzed by atomic absorption spectrometry (AAS Perkin Elmer AAnalyst 200). The amount of metal adsorbed ( $q$ , mg Cd g<sup>-1</sup>) was calculated by the mass balance equation:  $q = V(C_0 - C_{eq})/m$ , where  $C_0$  and  $C_{eq}$  (mg Cd L<sup>-1</sup>) are the initial and equilibrium Cd(II) concentrations, respectively.

Several sorption kinetic experiments were performed by contact under agitation of a fixed amount of SIR (loading in the range 99–416 mg extractant g<sup>-1</sup>) with a fixed volume ( $m/V$ : 4 g L<sup>-1</sup>) of 1 M HCl solution containing varying Cd(II) concentrations (in the range 60–200 mg Cd(II) L<sup>-1</sup>). In order to compare the different lots of SIR on the same basis of reactive groups, a series of kinetics was performed adjusting the amount of SIR to fix the amount of Cyphos® IL-101 at the value of about 800 mg per L of solution ( $C_0$ : 100 mg Cd L<sup>-1</sup>). A complementary series of kinetics was performed adjusting the amount of SIR to obtain the same Cd(II) concentration at equilibrium. Temperature was varied in the range 10–40 °C. Detailed experimental conditions are reported in the caption of the figures. Samples were collected at fixed times and analyzed for determination of residual metal concentrations.

For the study of Cd(II) desorption, an amount of 100 mg of SIR (extractant loading: 416 mg IL g<sup>-1</sup>) was mixed with 25 mL of Cd(II) solution (1 M HCl solution, initial metal concentration: 100 mg Cd(II) L<sup>-1</sup>) for 24 h. The residual concentration measured by AAS after filtration served to determine the amount of metal bound to the resin. The metal-loaded resin was mixed for 24 h with 25 mL of a series of eluents: water, 0.1 M Na<sub>2</sub>SO<sub>4</sub>, 0.1 M HNO<sub>3</sub>, 0.1 M H<sub>2</sub>SO<sub>4</sub>. After filtration the metal concentration in the eluent was determined by AAS in order to obtain the amount of Cd desorbed from the resin. The amount of metal desorbed divided by the amount of metal bound to the SIR served for calculating the desorption yield (or efficiency). For the evaluation of sorption/desorption cycles, the same procedure was used for five cycles.

### 3. Results and discussion

#### 3.1. Resin characterization

##### 3.1.1. Resin impregnation

Ten lots of resins were prepared with increasing concentrations of IL (from 25 to 579 mg IL g<sup>-1</sup>; i.e., 0.048–1.115 mmol IL g<sup>-1</sup>). Fig. 1 shows the IL content in the resin in function of the amount of IL used in the impregnation solution (given for a standard amount of resin of 10 g). The experimental data (experimental points) are compared to the “theoretical” curve (which represents for each resin the total immobilization of the IL). This curve shows that under selected experimental conditions (concentration range) the IL was completely absorbed in the porous network of the resin.

##### 3.1.2. Optical microscopy

Fig. 2 shows optical microphotographs for a selection of SIRs (compared to the raw resin). As the amount of IL immobilized on the resin increases a substantial change in the aspect of the SIRs is observed: raw resin is translucent, when the resin is loaded with increasing amounts of IL the beads become opaque. However, at the higher IL loading (L10) a new change in the aspect of the beads

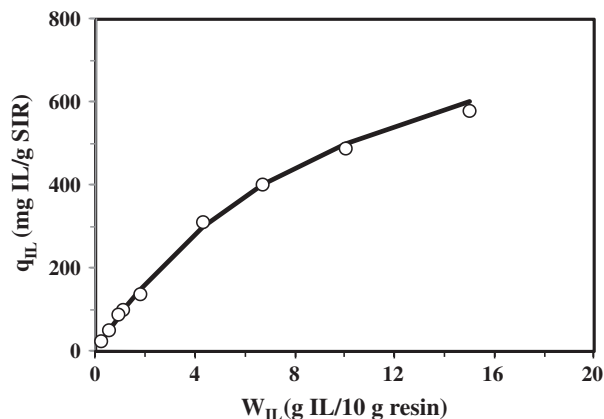


**Fig. 1.** Resin impregnation (amount of IL immobilized in the resin,  $q_{IL}$ , in function of the amount of IL used for resin impregnation,  $W_{IL}$ ). Symbols represent experimental data and solid line represents the theoretical curve considering the amount of IL used in the impregnation solution.

appears: the resins become again translucent and even almost transparent.

##### 3.1.3. Textural analysis

The observation of the SIRs made interesting a more specific analysis of the surface properties of these materials. Nitrogen adsorption/desorption isotherms were carried out for the different SIR lots (see Additional Material, Fig. AM1). And these data were used for calculating the pore size and the specific surface area (Fig. 3a), as well as the pore volume (Fig. 3b). As the IL content increased the apparent size of the pores increased, while the specific surface area (SSA) drastically decreased. The IL filled the smallest mesopores (<40 Å) of the resin leading to a predominance of largest mesopores (40–400 Å) (see Additional Material, Fig. AM2: Effect of IL loading on the distribution of pore sizes). The filling of mesopores logically resulted in a decrease of the SSA. At very high loading (i.e., 487 mg IL g<sup>-1</sup>), the SSA was close to 20 m<sup>2</sup> g<sup>-1</sup>. At the highest loading (i.e., at 579 mg IL g<sup>-1</sup>), the SSA was not represented (due to inaccuracies in the determination of the SSA); however, the SSA tended to a few m<sup>2</sup> g<sup>-1</sup>. This means that the internal porosity was almost completely filled and the SSA, under these conditions, only corresponded to the external surface area of the resin beads. The density of IL is supposed to be close to 0.9 g mL<sup>-1</sup> (Cytec data), based on the pore volume of Amberlite XAD-7 (Table 1), this means that the amount of IL that can be bound in the porous network can reach up to 0.9 g IL per g of Amberlite XAD-7 (or 1.7 mmol IL g<sup>-1</sup>), or 0.47 g IL per g of SIR. This is slightly lower than the levels reached in the impregnation of the resin: this can be probably attributed to the swelling of the resin.

The pore volume linearly decreased with increasing IL loading (Fig. 3b). The projection of the curve for the highest loading (not shown on the figure) would approach 0 mL g<sup>-1</sup>. This is consistent with previous observations (specific surface area) and the hypothesis of full saturation of the porous network.

Fig. 4 shows a schematic view of the resin in its free form (A) and with different IL loading (B–E) (see Additional Material, Fig. AM2, for supporting information on the evolution of the size

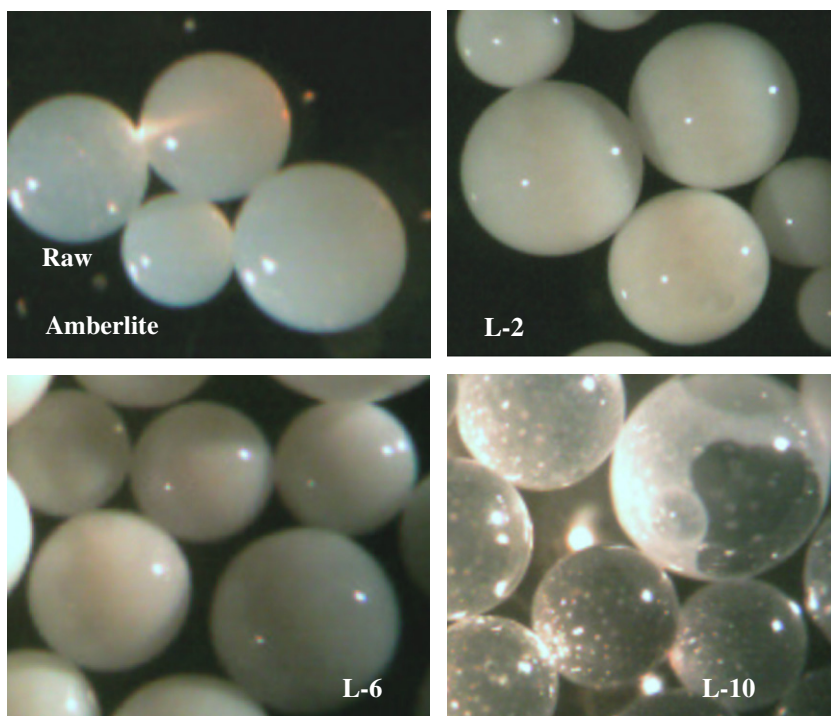


Fig. 2. Optical microscope photographs in function of resin loading (raw resin; L2 –  $q_{IL}$ : 50 mg IL  $g^{-1}$  SIR; L6 –  $q_{IL}$ : 193 mg IL  $g^{-1}$  SIR; L10  $q_{IL}$ : 579 mg IL  $g^{-1}$  SIR).

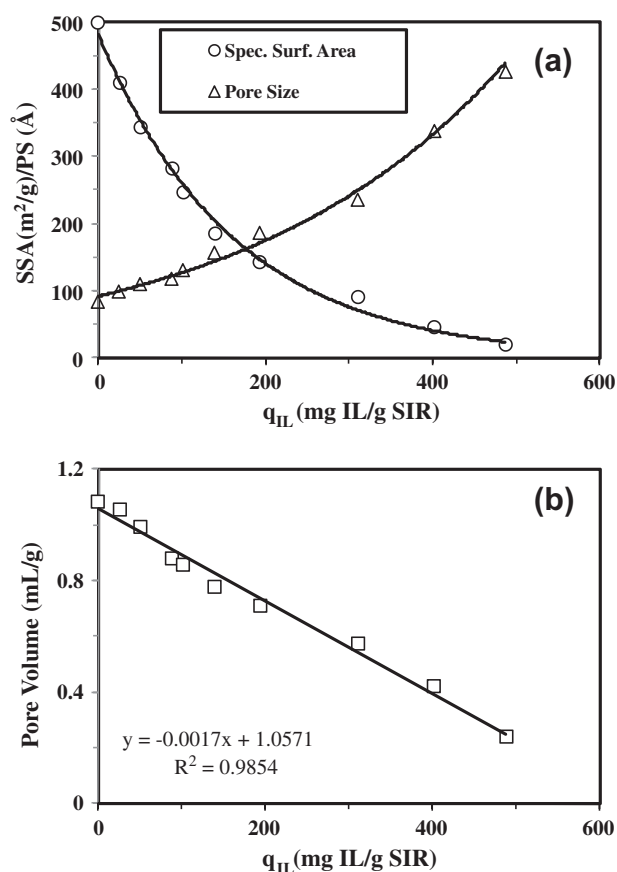


Fig. 3. Textural analysis of impregnated resins in function of IL loading (a: SSA: specific surface area ( $m^2 g^{-1}$ ); PS: pore size ( $\text{\AA}$ ); b: pore volume ( $mL g^{-1}$ )).

of the pores with increasing IL loading). The IL initially forms (at low IL loading) a thin layer at the internal surface of the resin

(B). At intermediary IL loading, the extractant loading fills the smallest mesopores ( $<40 \text{\AA}$ ) (C). At high IL loading, the extractant progressively fills the intermediary mesoporous network (40–200  $\text{\AA}$ ) (D) and then the biggest pores ( $>200 \text{\AA}$ ). At the highest IL loading (E) the porous network is completely filled and the excess of IL remains bound on the external surface of the resins. This is consistent with the observations made on specific surface area: increasing the IL content caused a significant decrease in the surface available for interacting with the solution.

#### 3.1.4. SEM-EDAX analysis

Amberlite XAD-7 (the support), Amberlite XAD-7 impregnated with Cyphos<sup>®</sup> IL-101 (the SIR) and Cd-loaded SIR were analyzed using an environmental scanning electron microscope coupled with an energy dispersive X-ray microanalysis system (ESEM-EDAX). Fig. 5 shows the cross-section view of the resins together with the cartography of target elements. The distribution of C and O elements on Amberlite XAD-7 shows that the supporting resin is homogeneous. The ESEM-EDAX analysis of P and Cl elements (the tracers of the presence of the IL) shows that the SIRs were homogeneously filled for an IL loading close to 400 mg IL  $g^{-1}$ . The same analysis was performed on a SIR loaded with 100 mg IL  $g^{-1}$  (i.e., much under saturation conditions) and a similar trend was observed: P element was homogeneously distributed (no gradient of concentration; image not shown). After Cd(II) sorption, the homogeneous distribution of the metal in the whole mass of the resin indicates that reactive groups are accessible even at the center of the particle (shown for the SIR loaded with 400 mg IL  $g^{-1}$  but this was also observed for an IL loading of 100 mg IL  $g^{-1}$ ; image not shown).

### 3.2. Sorption studies

#### 3.2.1. Influence of HCl concentration

Fig. 6 shows the influence of HCl concentration on Cd(II) sorption efficiency for the different lots of s. Raw Amberlite XAD-7,

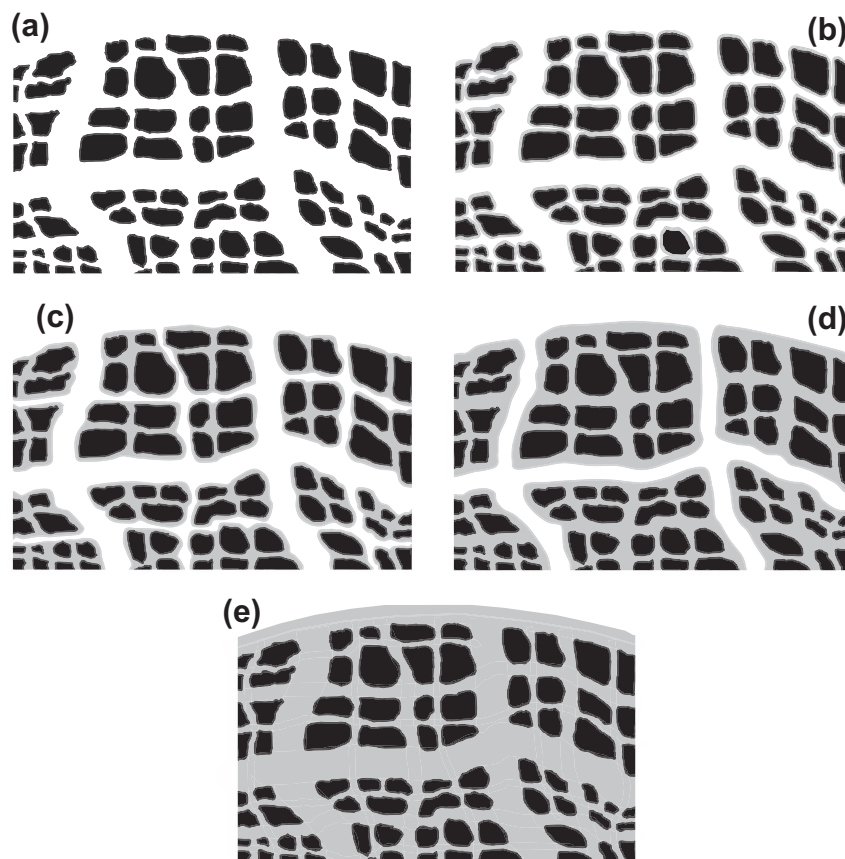
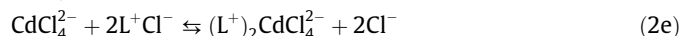
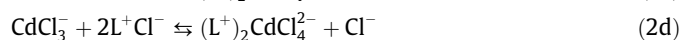


**Fig. 4.** Schematic representation of the porous network of Amberlite XAD-7 loaded with increasing amounts of Cyphos IL-101 – a: Raw Amberlite XAD-7 resin; b: low IL loading (covering of surface with a thin film of IL); c: intermediary IL loading (smallest mesopores, around <40 Å, are completely filled; the surface of mesopores is covered with IL but space remains available for access of the aqueous solution to this porous network and interfacial area progressively diminish); d: the intermediary and biggest mesopores are progressively filled with IL; the volume accessible for aqueous solution decreases; e: the porous volume is completely filled with the IL.

without IL impregnation, adsorbed negligible amounts of Cd(II): at HCl concentration below 1 M, Cd(II) was not adsorbed; above 1 M, sorption efficiency slightly increased but remained systematically lower than 6%. The sorption may result from the reaction of Cd(II) species with the resin that was partially hydrolyzed by the strong acid media. Several studies have shown that in strong acid solutions, the acrylic resins bearing ester groups (such as Amberlite XAD-7) can bind small amounts of metal cations as chloroanionic complexes through interaction with the oxygen of partly hydrolyzed ester groups [33,49–52].

A detailed observation of the curves shows that in the first part of the curve (below 0.5–2 M) the sorption efficiency increased with HCl concentration, while above 1–2 M the sorption efficiency decreased; the limit between the increasing and decreasing sections depended on IL loading. These results can be, at least partly, explained by the impact of Cd(II) speciation in HCl solutions. Actually, in HCl solutions, Cd(II) can form a series of complexes:  $\text{CdCl}^+$ ,  $\text{CdCl}_2$ ,  $\text{CdCl}_3^-$  and  $\text{CdCl}_4^{2-}$ . The expected mechanism for the extraction of metal ions by Cyphos ILs in HCl solutions has been previously described in solvent extraction [40,41], and in sorption processes with Cyphos® IL-101 immobilized in biopolymer capsules or synthetic resins [32–39]. Metal cations form with chloride ions chloroanionic complexes that bound to tetraalkylphosphonium cations. The variation in the distribution of Cd(II) species with HCl concentration may explain the observations summarized in Fig. 6. At low HCl concentration (below 0.8 M) Cd(II) is essentially present under the form of neutral ( $\text{CdCl}_2$ ) or cationic species

( $\text{CdCl}^+$ ); anionic species ( $\text{CdCl}_3^-$  and  $\text{CdCl}_4^{2-}$ ) begin to predominate only above 0.8 M (see Additional Material, Fig. AM3). The proportion of adsorbable species increased with HCl concentration, consistently with experimental data. Above 2 M HCl concentration the proportion of  $\text{CdCl}_3^-$  begins to decrease and  $\text{CdCl}_4^{2-}$  begins to predominate above 5 M HCl concentration. The decrease in sorption efficiency above 2–4 M HCl concentration results from the increasing concentration of  $\text{CdCl}_4^{2-}$  and of chloride anions (excess of chloride anions). The possible interactions between the IL and Cd(II) species are reported in the following equations:



where  $\text{L}^+$  represents the phosphonium cation ( $\text{P R}_3\text{R}^+$ ) and  $(\text{L}^+)_2\text{CdCl}_4^{2-}$  represents extracted Cd(II) species (as the anionic chloroanionic complex bound to phosphonium cation).

At low HCl concentrations ( $\leq 1$  M), an increase of chloride ion concentration improves the formation of the complex  $(\text{L}^+)_2\text{CdCl}_4^{2-}$  (Eqs. (2a) and (2b)); this explains that in the first section of the curves the sorption efficiency increases with HCl concentration. In the intermediary HCl concentration range (i.e., 1–5 M)  $\text{CdCl}_3^-$  is the predominant species in aqueous solution and Equation 2d is

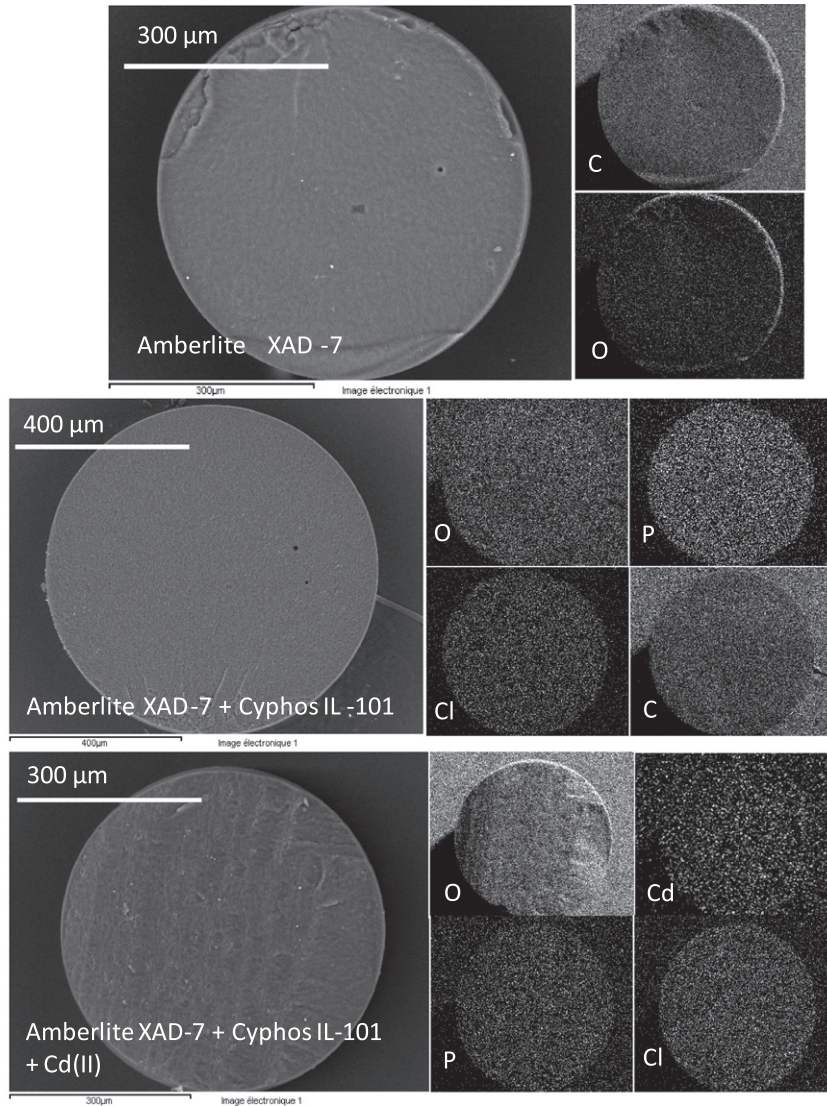


Fig. 5. SEM-EDAX analysis of Amberlite XAD-7, SIR (Amberlite XAD-7 + Cyphos IL-101) and SIR after Cd(II) sorption ( $q_{IL}$ : 416 mg IL  $g^{-1}$  SIR).

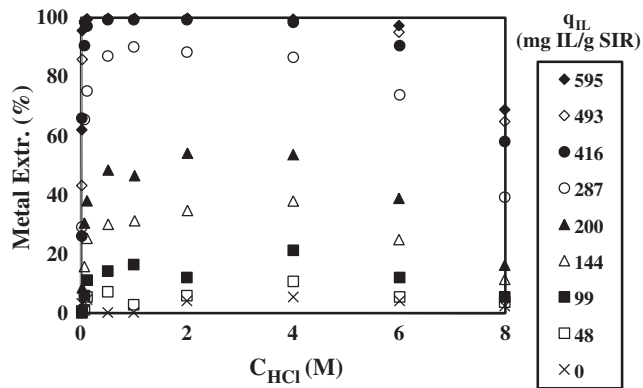


Fig. 6. Influence of HCl concentration and IL loading on Cd(II) extraction ( $T$ : 20 °C; agitation: 24 h at 150 rpm;  $C_0$ : 100 mg Cd  $L^{-1}$ ; sorbent dosage, SD: 4 g  $L^{-1}$ ).

bigger impact for destabilizing the complex and the sorption efficiency significantly decreases. In the case of Zn(II) sorption using the same SIR, Gallardo et al. [32] concluded that Zn(II) is extracted by the Cyphos® IL-101 as the species  $(L^+)_2ZnCl_4^{2-}$ .

### 3.2.2. Sorption isotherms

The shape of the isotherm curves was not affected by the IL content (Fig. 7): (a) the curves are characterized by a sharp initial curve that indicates that the resin has a strong affinity for Cd(II) ions, (b) the saturation is reached for a residual concentration has low as 20 mg Cd  $L^{-1}$ . The saturation plateau suggests that the distribution of Cd(II) at equilibrium between liquid ( $C_{eq}$ , mg Cd  $L^{-1}$ ) and solid ( $q_m$ , mg Cd  $g^{-1}$ ) phases will be governed by the Langmuir equation:

$$q = \frac{q_m b C_{eq}}{1 + b C_{eq}} \quad (3)$$

where  $b$  (affinity coefficient,  $L \text{ mg}^{-1}$ ) and  $q_m$  (sorption capacity at monolayer saturation,  $\text{mg g}^{-1}$ ) are the parameters of the model. The parameters of the Langmuir equation are summarized in Table 3 (the continuous lines in Figs. 7 and 9 show the modeling of experimental data with the Langmuir equation and the parameters listed

the representative reaction. A chloride ion is exchanged so that the extraction efficiency slightly diminishes. For the highest HCl concentration ( $>5 \text{ M}$ ),  $CdCl_4^{2-}$  is the predominant species and two chloride ions are exchanged (Eq. (2e)). Chloride concentration has a

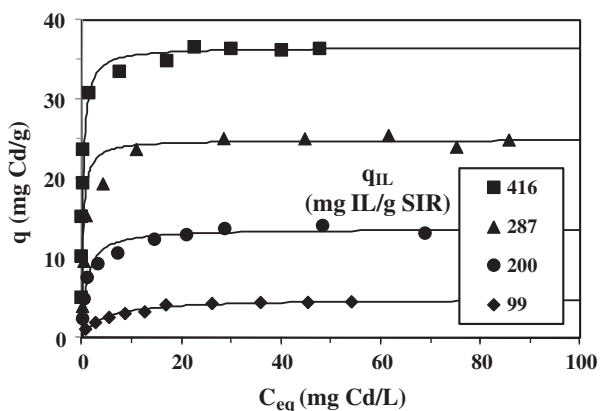


**Fig. 7.** Cd(II) sorption isotherms in 1 M HCl solutions (solid lines: modeling of isotherms with the Langmuir equation) – influence of IL loading ( $T$ : 20 °C; agitation: 24 h at 150 rpm; sorbent dosage, SD: 4 g L<sup>-1</sup>).

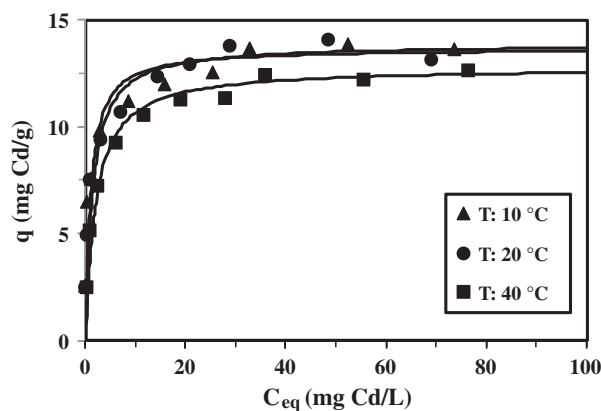


**Fig. 9.** Cd(II) sorption isotherms in 1 M HCl solutions (solid lines: modeling of isotherms with the Langmuir equation) – influence of temperature (agitation: 24 h at 150 rpm;  $q_{IL}$ : 200 mg IL g<sup>-1</sup> SIR; sorbent dosage, SD: 4 g L<sup>-1</sup>).

**Table 3**  
Sorption isotherms – parameters of the Langmuir equation.

IL loading <sup>*</sup> (mg IL g <sup>-1</sup> )	$T$ (°C)	$q_m^{**}$ (mg Cd g <sup>-1</sup> )	$b$ (L mg <sup>-1</sup> )	$R^2$	IL/Cd(II)
99 [0.191]	20	4.89 [0.0435]	0.228	0.997	4.4
200 [0.385]	20	13.71 [0.122]	0.999	0.998	3.2
287 [0.553]	20	24.89 [0.221]	3.42	0.999	2.5
416 [0.801]	20	36.57 [0.325]	3.45	1.000	2.5
200 [0.385]	10	13.90 [0.124]	0.744	0.999	3.1
200 [0.385]	40	12.82 [0.114]	0.508	0.999	3.4

<sup>\*</sup> [mmol IL g<sup>-1</sup>].

<sup>\*\*</sup> [mmol Cd g<sup>-1</sup>]; IL/Cd(II): molar ratio between IL in the resin and Cd(II) at saturation of the SIR.

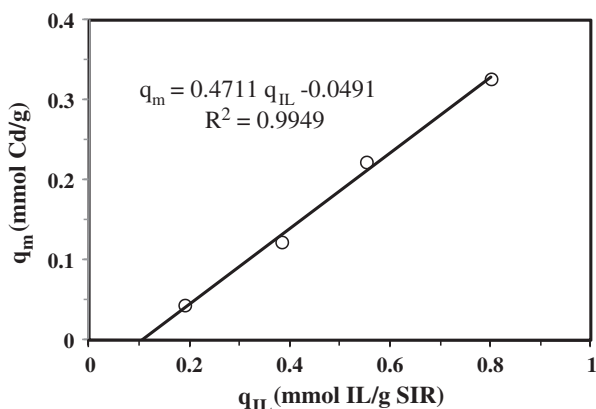


**Fig. 8.** Influence of IL loading on maximum sorption capacity (Langmuir constant) – Cd(II)/IL stoichiometric ratio.

in Table 3). The maximum sorption capacity logically increased with IL content. The affinity coefficient also increased with IL loading; this result contrasts with the results published by Saha et al. for Cr(VI) sorption on Amberlite XAD-7 loaded with Aliquat 336 [53], and by Benamor et al. [12], who impregnated Amberlite XAD-7 with di(2-ethylhexyl) phosphoric acid for Cd(II) sorption from HCl solutions. They concluded that the accessibility of reactive groups increased with extractant loading whereas the binding strengths of the functional groups decreased. In the present case both affinity and accessibility increased with IL loading. Additionally, the IL/Cd(II) molar ratio, at saturation, decreased when IL increased. This means that IL was more efficiently used when the porous

network was “densely” filled with the extractant. When IL loading decreased the arrangement of the IL in the porous network was less favorable to the binding of chloroanionic cadmium species. Fig. 8 shows the plot of sorption capacity versus the IL loading: the data are linearly distributed with a slope close to 0.5 (i.e., 0.47). This stoichiometric ratio indicates that two phosphonium cations were involved for the binding of one Cd(II) (probably under the form  $(L^+)_2CdCl_4^{2-}$ ), as a confirmation of the mechanism described by Eqs. (2a)–(2e).

This result could explain that the porous network should be well filled for optimizing the arrangement of the molecules of extractant to fit the interaction mode of the divalent anion. Additionally, a fraction of the IL immobilized in the resin remained inactive (negative ordinate intercept): this is probably related to a direct interaction of the IL with the polymer support (Amberlite XAD-7).

Sorption isotherms were obtained at different temperatures (Fig. 9). The curves obtained at 10 °C and 20 °C were almost overlapped, while a small shift was observed at 40 °C. Table 3 summarizes the parameters of the Langmuir equation: the sorption capacity at saturation of the monolayer ( $q_m$ ) decreased with increasing the temperature; however, the variation did not exceed 10%. The affinity coefficient did not follow a continuous trend: it reached a maximum at 20 °C; however, the variation was relatively weak (about 30% around the optimum value). The temperature, at least in the range 10–40 °C, did not significantly impact the sorption behavior of Cd(II) with Cyphos® IL-101 impregnated Amberlite XAD-7.

### 3.2.3. Influence of the composition of the solution

The treatment of spent batteries or waste materials, after mechanical treatment and magnetic separation frequently involves a leaching treatment in acidic solutions [54]. This acidic treatment induces the simultaneous leaching of different metal ions: the most frequent being Fe(III), Ni(II), Co(II) apart of Cd(II). Two kinds of acids can be used: HCl and H<sub>2</sub>SO<sub>4</sub> (in single solutions or binary solutions). For this reason, a series of experiments have been performed in order to measure the impact of the acid and of the presence of competitor metals on Cd(II) recovery. Fig. 10a shows the recovery of Fe(III), Cd(II), Ni(II) and Co(II) (at equimolar concentration) in different HCl concentration solutions (0.001–8 M). Ni(II) and Co(II) ions were not adsorbed whatever the acid concentration. This is probably due to the fact that these metals do not form anionic complexes with chloride ions: their charge is not favorable to electrostatic attraction/ion exchange. The case is different for Fe(III) that forms a chloroanionic complex in concentrated HCl

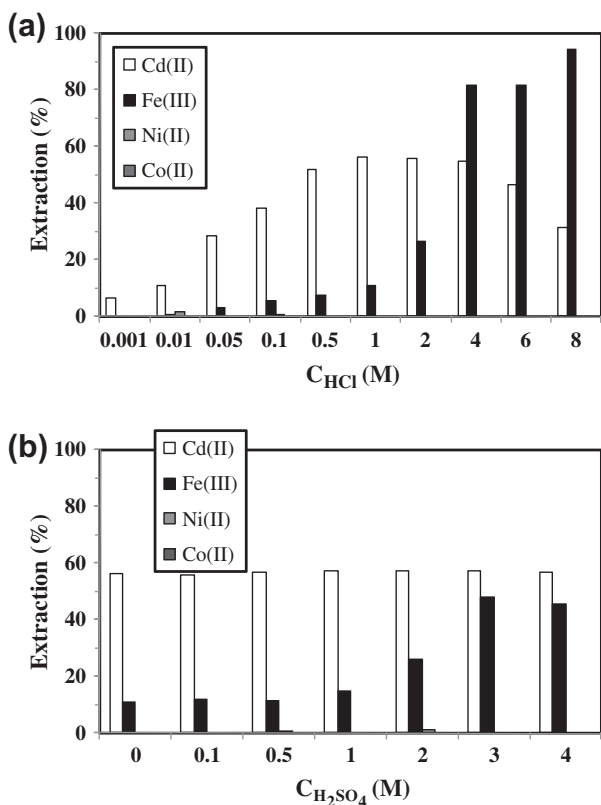


**Fig. 10.** Influence of the composition of the solution on Cd(II) sorption: (a) influence of the presence of Fe(III), Ni(II) and Co(II) (impact of HCl concentration); (b) influence of the presence of Fe(III), Ni(II) and Co(II) in 1 M HCl solution and the addition of sulfuric acid at increasing concentrations (agitation: 24 h at 150 rpm;  $q_{IL}$ : 200 mg IL  $g^{-1}$  SIR; sorbent dosage, SD: 4  $g L^{-1}$ ; metal concentration:  $8.9 \times 10^{-4}$  M).

solutions (above 2 M; see Additional Material, Fig. AM4). For this reason Fe(III) can be removed from acidic solutions at concentration above 2 M, these competitor anions induce a decrease of Cd(II) sorption since both Cd(II) and Fe(III) anionic species compete for the same binding sites (i.e.,  $R_3R'P^+$ ). The sorption of Cd(II) increased with HCl concentration as shown in previous sections and the presence of other metals did not significantly interfere at low HCl concentration (below 2 M); above 2 M HCl concentration the chloroanionic Fe(III) species caused a progressive decrease of Cd(II) binding.

In 1 M HCl solutions, the addition of increasing amounts of sulfuric acid (between 1 and 4 M) did not change the sorption of Cd(II) (Fig. 10b), that remained in the whole concentration range around 60%. Ni(II) and Co(II) were not adsorbed for the same reasons as above: these metal ions do not form anionic complexes that could bind to tetraalkyl phosphonium cation. The dissociation of the acid (formation of  $HSO_4^-$ ) did not influence Cd(II) sorption. The sorption of Fe(III) occurs on the complete sulfuric acid concentration range at the level reached with 1 M HCl solution (Fig. 10a); however, when sulfuric acid concentration increased above 2 M, the sorption efficiency increased again up to 45–48%. This increase is less than the levels reached with HCl at comparable concentrations (proton and dissociated anion): the formation of Fe(III) sulfate complexes does not exceed 10% (calculations made with Medusa software [55]) contrary to chloroanionic complexes that can reach up to 50% in 8 M HCl solutions. This small increase in the proportion of anionic Fe(III) sulfate complexes (added to chloroanionic complexes) may explain that the impact of sulfuric acid on the sorption efficiency of Cd(II) was almost no detectable.

Cyphos® IL-101 impregnated on Amberlite XAD-7 has a preference for Cd(II) over other base metals at HCl concentrations close to 1 M, the presence of sulfuric acid (a co-acid that could be present in the leaching of spent batteries and industrial wastes) did not significantly impact Cd(II) uptake efficiency. These preliminary results reveal that when “playing” with HCl concentration it is possible to roughly separate Cd(II) from Fe(III) and both metals totally from Ni(II) and Co(II).

### 3.2.4. Uptake kinetics

Uptake kinetics can be controlled by several mechanisms including resistance to mass transfer (i.e., film diffusion, intraparticle diffusion), chemical reaction rate. In most cases, binding in sorbents is controlled by diffusion mechanisms rather than the reaction rate; though some systems have been shown to be governed by a reaction mechanism in relation with the parallel ionic reactions (which change the speciation of the ions involved in the principal reaction). Since the pioneering work on dynamics of ion exchange processes by Streat [56], and Helfferich [57], Juang and Ju discussed a series of simplified modeling systems derived from the homogeneous diffusion model (HDM) and the shrinking core model (SCM) [58]. The HDM involves counterdiffusion of exchangeable species in quasi homogeneous media, with a contribution from film diffusion (HDM-FD) and/or particle diffusion (HDM-PD). Solute molecules and exchangeable species (immobilized on the resin) follow a similar diffusion mechanism (but in the opposite direction). In the case of the SCM, a sharp virtual boundary exists between the reacted shell of the particle and the unreacted core, and this boundary moves towards the center of the particle [59,60]. This model was developed with different systems depending on the controlling step: film diffusion (SCM-FD), particle diffusion (SCM-PD) and chemical reaction rate (SCM-CR) [58]. A number of mathematical equations have been developed to simulate these mechanisms, they are listed below:

#### Homogeneous diffusion model

$$\text{Film diffusion : } F_1(X) = -\ln(1 - X) = f(t) \quad (4)$$

$$\text{Particle diffusion : } F_2(X) = -\ln(1 - X^2) = f(t) \quad (5)$$

#### Shrinking core model

$$\text{Film diffusion : } G_1(X) = X = g\left(\int_0^t C(t) dt\right) \quad (6)$$

$$\text{Particle diffusion : } G_2(X) = 3 - 3(1 - X)^{2/3} - 2X = g\left(\int_0^t C(t) dt\right) \quad (7)$$

$$\text{Chemical reaction rate : } G_3(X) = 1 - (1 - X)^{1/3} = g\left(\int_0^t C(t) dt\right) \quad (8)$$

where  $X$  is the fractional approach to equilibrium (i.e.,  $q(t)/q_{eq}$ ), the amount adsorbed at time  $t$  divided by the amount of metal adsorbed at equilibrium. Plotting  $F_i$  and  $G_i$  functions versus time and the integral term (respectively) determined the most appropriate mechanism for describing the controlling step. The curve giving a straight line (good correlation measured by the correlation coefficient) is assumed to be the predominant limiting step. Examples of models testing are presented as Additional Material (Figs. AM5 and AM6). At low IL loading (Fig. AM4) the models that best fit experimental data were related to intraparticle diffusion: both HDM and SCM gave good fit of experimental data, only physical observations such as SEM-EDAX analysis in the transient state could give indication on the prevalent model. At higher IL loading (Fig. AM5) the selection of the best equation became more difficult

indicating that several mechanisms could be involved in the control of uptake kinetics (including intraparticle diffusion and chemical reaction).

The intraparticle diffusion coefficient ( $D_e$ , effective diffusivity,  $\text{m}^2 \text{min}^{-1}$ ) was determined using Crank's equation, assuming the solid to be initially free of metal, and the kinetics to be controlled by intraparticle diffusion resistance [61]:

$$\frac{q(t)}{q_{eq}} = 1 - \sum_{n=1}^{\infty} \frac{6\alpha(\alpha + 1) \exp\left(\frac{-D_e q_n^2 t}{r^2 \alpha^2}\right)}{9 + 9\alpha + q_n^2 \alpha^2} \quad (9)$$

$q(t)$  and  $q_{eq}$  are the concentrations of the metal in the resin at time  $t$  and equilibrium, respectively,  $r$  is the radius of the particle (275  $\mu\text{m}$ ), and  $q_n$  non-zero roots of the equation:

$$\tan q_n = \frac{3q_n}{3 + \alpha q_n^2} \quad (10)$$

with

$$\frac{q}{VC_o} = \frac{1}{1 + \alpha} \quad (11)$$

The Mathematica™ software was used for the determination of the intraparticle diffusion coefficient,  $D_e$ , and for the simulation of experimental data (represented by the continuous lines on the Figs. 11–14). Table 4 reports the intraparticle diffusion coefficients with different experimental conditions corresponding to the comparison of kinetics for resins prepared with different IL loadings (Fig. 11), different initial concentrations (Fig. 12) and for different sorbent dosages (SD) with constant amount of IL (Fig. 13).

**3.2.4.1. Influence of IL loading.** The experiments were performed with 100  $\text{mg Cd L}^{-1}$  solutions. For the resins prepared with IL loadings of 99 and 200  $\text{mg IL g}^{-1}$ , the experimental conditions correspond to the saturation of the resins (Fig. 11). The calculation of corresponding sorption capacities at equilibrium fit with maximum sorption capacities reported in Table 3 (with a variation less than 5%). The intraparticle diffusion equation fitted well experimental data and the equilibrium was reached within a few hours (2 and 4 h for IL loadings of 99 and 200  $\text{mg g}^{-1}$ , respectively). With the most loaded SIR (i.e., 416  $\text{mg IL g}^{-1}$ ), the experimental conditions did not reach the saturation of the resin (the sorption capacity at equilibrium was close to 25  $\text{mg Cd g}^{-1}$  versus 36.6  $\text{mg Cd g}^{-1}$ ). Plotting the fractional approach to equilibrium (FATE, see Additional Material, Fig. AM7a) versus time allows confirming these trends: the curves overlapped at low IL loading while the highest loaded SIR exhibited a distinct shape. Benamor et al. [12] obtained perfect superimposition of the FATE versus time curves for the sorption of Cd(II) using Amberlite XAD-7

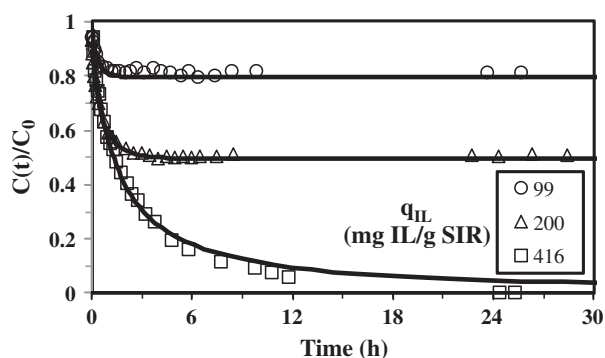


**Fig. 11.** Cd(II) uptake kinetics. Influence of IL loading at constant sorbent dosage ( $4 \text{ g L}^{-1}$ ).  $C_{\text{HCl}}$ : 1 M; Cd(II): 100  $\text{mg L}^{-1}$ ;  $T$ : 20 °C; solid lines: modeling of the kinetics with the intraparticle diffusion equation, Crank's equation).

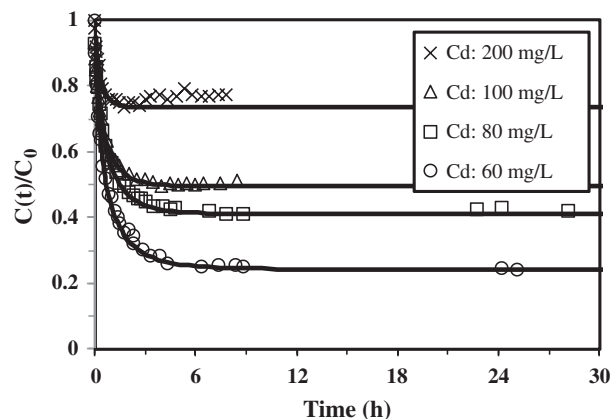


**Fig. 12.** Influence of initial metal concentration on Cd(II) uptake kinetics ( $C_{\text{HCl}}$ : 1 M;  $q_{\text{IL}}$ : 200  $\text{mg IL g}^{-1}$  SIR;  $T$ : 20 °C; sorbent dosage, SD: 4  $\text{g L}^{-1}$ ; solid lines: modeling of the kinetics with the intraparticle diffusion equation, Crank's equation).

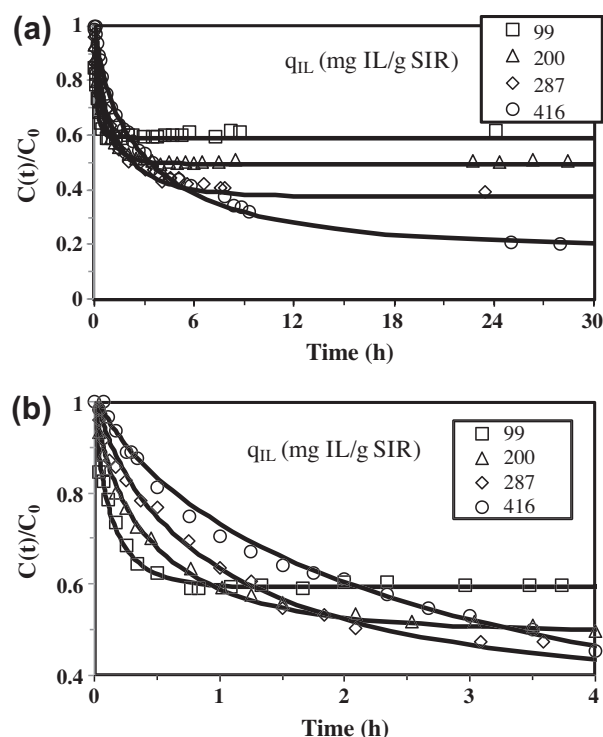


**Fig. 13.** Cd(II) uptake kinetics. Influence of IL loading varying sorbent dosage (SD) to obtain a constant IL amount ( $800 \text{ mg L}^{-1}$ ). ((a): complete kinetics; (b): initial section);  $q_{\text{IL}}$ : 99  $\text{mg IL g}^{-1}$  SIR (SD: 8  $\text{g L}^{-1}$ );  $q_{\text{IL}}$ : 200  $\text{mg IL g}^{-1}$  SIR (SD: 4  $\text{g L}^{-1}$ );  $q_{\text{IL}}$ : 287  $\text{mg IL g}^{-1}$  SIR (SD: 2.67  $\text{g L}^{-1}$ );  $q_{\text{IL}}$ : 416  $\text{mg IL g}^{-1}$  SIR (SD: 2  $\text{g L}^{-1}$ );  $C_{\text{HCl}}$ : 1 M;  $T$ : 20 °C;  $C_0$ : 100  $\text{mg Cd L}^{-1}$ ; solid lines: modeling of the kinetics with the intraparticle diffusion equation, Crank's equation).

impregnated with di(2-ethylhexyl) phosphoric acid (DEHPA). The differences in the experimental conditions were probably not large enough to give significant differences in the level of saturation of the resin, and then to make detectable the differences in the profiles. In their study, the differences were more marked when the pH was decreased. For the highest loaded SIR, the intraparticle diffusion equation fitted well experimental data and it is interesting to observe that the initial section of the curve (within the first 45 min of contact) was almost overlapped with that obtained with the intermediary IL loading (i.e., 200  $\text{mg IL g}^{-1}$  SIR). However, the time required to reach equilibrium was drastically increased (up

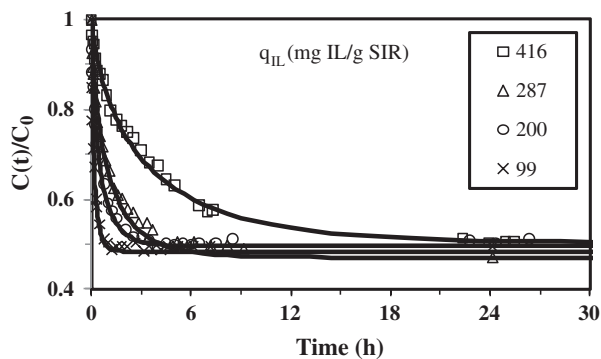


**Fig. 14.** Cd(II) uptake kinetics. Influence of IL loading varying sorbent dosage to obtain similar equilibrium metal concentrations.  $q_{IL}$ : 416 mg IL g<sup>-1</sup> SIR (SD: 1.27 g L<sup>-1</sup>);  $q_{IL}$ : 318 mg IL g<sup>-1</sup> SIR (SD: 2.21 g L<sup>-1</sup>);  $q_{IL}$ : 200 mg IL g<sup>-1</sup> SIR (SD: 4 g L<sup>-1</sup>);  $q_{IL}$ : 99 mg IL g<sup>-1</sup> SIR (SD: 11.4 g L<sup>-1</sup>);  $C_{HCl}$ : 1 M;  $T$ : 20 °C;  $C_0$ : 100 mg Cd L<sup>-1</sup>; solid lines: modeling of the kinetics with the intraparticle diffusion equation, Crank's equation).

**Table 4**  
Uptake kinetics – intraparticle diffusion coefficients (Crank's equation).

Temperature (°C)	IL (mg IL g <sup>-1</sup> resin)	$C_0$ (mg L <sup>-1</sup> )	SD (g L <sup>-1</sup> )	$D_e \times 10^{10}$ (m <sup>2</sup> min <sup>-1</sup> )
20	200	200	4	7.04
20	200	100	4	3.32
20	200	80	4	2.30
20	200	60	4	1.48
20	99	100	4	8.06
20	416	100	4	0.01
20	99	100	8	1.34
20	287	100	2.67	1.13
20	416	100	2	0.21
20	99	100	11.4	9.91
20	287	100	2.21	1.57
20	416	100	1.27	0.52
10	200	100	4	2.53
40	200	100	4	5.81

to 24 h) for an IL loading of 416 mg IL g<sup>-1</sup> SIR. This means that diffusion properties were substantially controlled by IL loading. This is confirmed by the comparison of the intraparticle diffusion coefficients that decrease with IL loading, moderately at intermediary IL content but dramatically at high IL content (Table 4). This evolution is consistent with the variations of the pore volume and specific surface area (summarized in Fig. 3). The progressive saturation of the porous network with the IL induces supplementary restrictions to intraparticle diffusion since the diffusivity of metal ions in organic phase is significantly lower to that in water. This contributes to reducing mass transfer performance when increasing IL loading. Moreover, the intraparticle diffusion coefficient increased linearly with specific surface area, may be due to a bigger interfacial surface available for reaction. This should be taken as an indicative trend since the comparison of the data was limited to three values of IL loading.

**3.2.4.2. Influence of metal concentration.** The concentration of Cd(II) was varied in the range 60–200 mg L<sup>-1</sup> (Fig. 12). Equilibrium was reached within 4–6 h: the time required to reach equilibrium slightly increased with decreasing metal concentration. Indeed, a greater gradient induces a driving force that improves mass transfer. Additionally, higher metal concentration allows reaching resin saturation faster. The plot of FATE versus time confirms this trend (see Additional Material, Fig. AM7b): at the highest metal concentration (i.e., 200 mg Cd L<sup>-1</sup>) the equilibrium is reached much faster than for other metal concentrations (the FATE curves

superimposed for concentrations varying between 60 and 100 mg Cd L<sup>-1</sup>). Crank's equation was successfully used for modeling experimental data. The intraparticle diffusion coefficient increases with metal concentration. This trend is contrary to the evolution observed by Benamor et al. [12] who observed that the intraparticle diffusion decreased with increasing Cd(II) concentration in the case of DEHPA-impregnated Amberlite XAD-7. Nestle and Kimmich [62] investigated the sorption of Cu with alginate gel beads and they correlated the concentration-dependent diffusion coefficients with the sorption isotherm that governed the distribution of the solute at equilibrium. For example, in the case of a system described by the Langmuir equation the intraparticle diffusion coefficient obeys the equation:

$$D = \frac{(1 + bC)^2}{(1 + bC)^2 + q_m b} D_0 \quad (12)$$

where  $D_0$  is the diffusion coefficient in the absence of any sorption reaction.

Using this equation for the experimental data did not allow linearizing the intraparticle diffusion coefficient with the equilibrium concentration: calculated values were not linearly distributed against intraparticle diffusion coefficient calculated from kinetic profiles. The order of magnitude of the intraparticle diffusion coefficient for Cyphos® IL-101 impregnated Amberlite XAD-7, i.e., 1.5–3.3 × 10<sup>-10</sup> m<sup>2</sup> min<sup>-1</sup>, is consistent with the values found for other SIRs: 3–5 × 10<sup>-10</sup> m<sup>2</sup> min<sup>-1</sup> for DEHPA-Amberlite XAD-7 [12], 3.2 × 10<sup>-10</sup> m<sup>2</sup> min<sup>-1</sup> for Cyanex 921-Amberlite XAD-7 [18], 0.01–1.2 × 10<sup>-10</sup> m<sup>2</sup> min<sup>-1</sup> for Cyanex 301-Amberlite XAD-7 (in phosphoric acid solutions) [14], and 3.1 × 10<sup>-10</sup> m<sup>2</sup> min<sup>-1</sup> for Amberlite XAD-2 impregnated with a bifunctional organophosphorous extractant (O-methyl-dihexyl-phosphine-oxide O'-hexyl-2-ethyl phosphoric acid) [20]. For Zn(II) sorption using Cyanex 921-Amberlite XAD-7, Navarro et al. found an intraparticle diffusion coefficient close to 0.3 × 10<sup>-10</sup> m<sup>2</sup> min<sup>-1</sup> [63]. Gallardo et al. [32] used the same system (Cyphos IL-101/Amberlite XAD-7) for the sorption of Zn(II); they observed that, contrary to Cd(II) binding, the increase in metal concentration tended to decrease the intraparticle diffusion coefficient from 5.9 × 10<sup>-11</sup> m<sup>2</sup> min<sup>-1</sup> to 2.7 × 10<sup>-11</sup> m<sup>2</sup> min<sup>-1</sup>. It is also interesting to compare the results obtained in this work with those reported by Blahušiak et al. [43] for butyric acid extraction into Amberlite XAD-1180 N impregnated with an ammonium ionic liquid (trialkylmethylammonium-bis(2,4,4-trimethylpentyl) phosphinate). Although these systems are very different, this case is interesting due to the higher intraparticle diffusion coefficient (10.7 × 10<sup>-10</sup> m<sup>2</sup> min<sup>-1</sup>). This value may be probably attributed to the superior textural characteristics of XAD-1180N: surface area (>450 m<sup>2</sup> g<sup>-1</sup>), pore diameter (average 300 Å) and pore volume (1.4 mL g<sup>-1</sup>) compared with those of XAD-7 (Table 1).

**3.2.4.3. Uptake at constant amount of IL.** A complementary experiment was performed using a constant amount of IL; in this case the sorbent dosage and the loading of IL were simultaneously varied. Fig. 13 shows the profiles obtained with a constant dosage of IL (i.e., 800 mg IL L<sup>-1</sup>, detailed experimental conditions are reported in the caption of the figure). Despite a constant amount of IL the residual concentration in the solution strongly varied with experimental conditions. At high IL loading in the SIR (low sorbent dosage) the sorption was much more efficient: the sorption efficient approached 80% contrary to the case of low IL loading (high sorbent dosage) where the sorption did not exceed 40%. This is consistent with previous observations on the effect of IL loading on SIR sorption isotherms: a part of the IL is tightly bound to the support; this fraction being non-reactive for Cd(II) binding. The fraction of IL bound to the support represents a higher percentage

**Table 5**  
Cd(II) desorption and IL-impregnated resin recycling.

Eluent	Cycle number	Extraction (%)	Desorption 1st step (%)	Desorption 2nd step (%)	Total desorption (%)
HNO <sub>3</sub> (0.1 M)	1	99.7	>99	0.7	100
	2	99.7	98.8	0.9	99.7
	3	99.7	96.5	0.6	97.1
	4	99.7	98.0	0.9	98.9
	5	99.4	>99	0.7	100
H <sub>2</sub> SO <sub>4</sub> (0.1 M)	1	99.7	87.6	15.0	100
	2	99.7	98.9	5.4	100
	3	99.7	90.3	7.7	98.0
	4	99.7	91.8	8.1	99.9
	5	99.6	81.1	1.9	83.0
Na <sub>2</sub> SO <sub>4</sub> (0.1 M)	1	99.7	68.9	34.7	100
	2	99.6	80.6	21.5	100
	3	99.5	84.4	15.0	99.4
	4	99.5	87.5	13.0	100
	5	98.4	86.0	17.6	100
H <sub>2</sub> O	1	99.7	8.0	56.7	64.7
	2	97.1	24.7	43.8	68.5
	3	94.8	24.5	42.7	67.2
	4	91.5	28.4	41.7	70.1
	5	93.0	21.0	41.6	62.6

of the IL for low IL loadings than for saturated SIRs and the total amount of metal that can be bound decreases. The second information obtained from these kinetic profiles concerns the initial slope of the kinetic curves (Fig. 13b). The slope decreased with increasing IL loading and decreasing sorbent dosage. Increasing IL loading, resin pores progressively are filled, interfacial area diminishes and IL film thickness on the resin is increased introducing a greater resistance to metal ion diffusion. Table 4 reports the intraparticle diffusion coefficients  $D_e$  obtained under these experimental conditions. The coefficient decreased (from  $3.32 \times 10^{-10}$  to  $0.21 \times 10^{-10} \text{ m}^2 \text{ min}^{-1}$ ) when increasing IL loading (between 200 and 416 mg IL g<sup>-1</sup>).

These experimental conditions result in different levels of IL saturation. A complementary experiment was performed with the objective of reaching the same levels of IL/Cd binding (Fig. 14). The equilibrium concentration was roughly the same (around 50 mg Cd L<sup>-1</sup>). The initial slope of the curve strongly increased with diminishing the IL loading (high amount of SIR): this corresponds again to a decrease in the IL film thickness and an increase in the interfacial surface available for reaction. The intraparticle diffusion coefficient linearly increased with the amount of SIR ( $R^2 = 0.999$ ) and specific surface area ( $R^2 = 0.989$ ).

**3.2.4.4. Effect of temperature.** Uptake kinetics were weakly affected by varying the temperature between 10 °C and 40 °C (see Additional Material, Fig. AM8): the curves almost overlap. However, Table 4 shows that the intraparticle diffusion coefficient increases with the temperature. This variation can be correlated to the change in the viscosity of the IL with temperature. Actually, the viscosity of Cyphos® IL-101 progressively decreases with dissolving a solute (water, hexane, for example) and with increasing the temperature (Cytec data). The decrease in viscosity improves the mobility of metal ions in the organic phase and the mass transfer properties are enhanced: the intraparticle diffusivity increased from  $2.53 \times 10^{-10} \text{ m}^2 \text{ min}^{-1}$  to  $5.81 \times 10^{-10} \text{ m}^2 \text{ min}^{-1}$  when temperature increased from 10 °C to 40 °C.

### 3.2.5. Desorption and resin recycling

The desorption of Cd(II) from loaded sorbents have been tested using four eluents (nitric acid, sulfuric acid and sodium sulfate at the same concentration, i.e., 0.1 M, and water). In order to evaluate the possibility to recycle the sorbent, five sorption/desorption

cycles were performed (Table 5). In each cycle, one extraction and two desorption steps were performed. Cadmium sorption remained stable over the five cycles when using nitric acid, sulfuric acid and sodium sulfate while with water a small decrease in sorption efficiency was observed. The complete desorption was achieved when using nitric acid, sulfuric acid and sodium sulfate for the five cycles while with water the desorption did not exceed 60–70%. However, these desorption yield were obtained in two successive desorption steps except for nitric acid. Indeed, in the case of nitric acid a single step was sufficient (desorption yield reached 99%). The eluents can be classified according: HNO<sub>3</sub> > H<sub>2</sub>SO<sub>4</sub> >> Na<sub>2</sub>SO<sub>4</sub> >> H<sub>2</sub>O.

These results confirm that the Cyphos® IL-101/Amberlite XAD-7 resin allows efficiently binding Cd(II) with high levels of metal recovery and efficient resin recycling for at least five cycles.

## 4. Conclusions

Immobilizing Cyphos® IL-101 in Amberlite XAD-7 allowed preparing SIRs that are very efficient for Cd(II) binding in HCl solutions. The optimum HCl concentration depends on IL loading but in most cases sorption reaches a maximum for HCl concentrations in the range 3–4 M. The maximum sorption capacity was correlated to IL loading: the stoichiometric ratio Cd(II)/IL is close to 0.5. Binding proceeds through an electrostatic attraction/ion exchange mechanism involving the reaction between chloroanionic Cd species (mainly CdCl<sub>4</sub><sup>2-</sup>) and phosphonium cation (R<sub>3</sub>R'P<sup>+</sup>). The presence of metal cations affects Cd(II) sorption only when the competitor metal forms anionic species that can compete with chloroanionic cadmium species. It is important to report that a part of the IL tightly bound to the polymer matrix does not react with metal ions. This “inactive” fraction has to be taken into account in the interpretation of sorption performance (equilibrium and kinetic performance).

Uptake kinetics are controlled by the resistance to intraparticle diffusion. The intraparticle diffusion coefficient increases with increasing metal concentration (increase of the concentration gradient), and temperature (decrease of IL viscosity in the porous network). The amount of IL in the porous network controls SIR specific surface area (interfacial area), IL film thickness, and then the diffusion of the metal in the SIR (slower diffusion in the organic phase than in the aqueous phase). At high IL loading the

intraparticle diffusion coefficient was drastically reduced by two orders of magnitude. Adjusting the sorbent dosage (with different IL loadings) to reach the same IL amount did not allow reaching the same equilibrium metal concentration. This is the confirmation that a fraction of IL bound to the resin remains inactive. The intraparticle diffusivity decreases with increasing IL loading (decreasing sorbent dosage). Adjusting the sorbent dosage (with different IL loadings) to reach the same equilibrium concentration shows that the initial slope of the kinetics increased with sorbent dosage. The intraparticle diffusivity linearly increased with sorbent dosage and interfacial area.

Cadmium adsorbed on SIR can be easily removed using several eluents. The SIR can be recycled for at least five cycles. Taking into account the extraction efficiency and the desorption efficiency (and the number of desorption required to achieve complete desorption) the eluents were ranked according  $0.1 \text{ M HNO}_3 > 0.1 \text{ M H}_2\text{SO}_4 \gg 0.1 \text{ M Na}_2\text{SO}_4 \gg \text{water}$ .

## Acknowledgments

Authors thank the Franco-Mexican PCP Program (Post-graduate Cooperation Program PCP No. 06/05) and the University of Guanajuato (CIAI 107/08 and 122/10) for financial support.

## Appendix A. Supplementary material

Supplementary data associated with this article can be found, in the online version, at [doi:10.1016/j.reactfunctpolym.2011.07.008](https://doi.org/10.1016/j.reactfunctpolym.2011.07.008).

## References

- [1] E. Rudnik, M. Nikiel, *Hydrometallurgy* 89 (2007) 61–71.
- [2] B.R. Reddy, D.N. Priya, *J. Power Sources* 161 (2006) 1428–1434.
- [3] C. Cerruti, G. Curutchet, E. Donati, *J. Biotechnol.* 67 (1998) 209–219.
- [4] F. Wang, L.-J. Wang, J.-S. Li, X.-Y. Sun, W.-Q. Han, *Trans. Nonferrous Met. Soc. China* 19 (2009) 740–744.
- [5] K. Bedoui, I. Bekri-Abbes, E. Srasra, *Desalination* 223 (2008) 269–273.
- [6] A. Demirbas, E. Pehlivan, F. Gode, T. Altun, G. Arslan, *J. Colloid Interf. Sci.* 282 (2005) 20–25.
- [7] A.H. Hawari, C.N. Mulligan, *Bioresour. Technol.* 97 (2006) 692–700.
- [8] M.S. Dzul Erosa, T.I. Saucedo Medina, R. Navarro Mendoza, M. Avila Rodriguez, E. Guibal, *Hydrometallurgy* 61 (2001) 157–167.
- [9] C. Moreno-Castilla, M.A. Alvarez-Merino, M.V. Lopez-Ramon, J. Rivera-Utrilla, *Langmuir* 20 (2004) 8142–8148.
- [10] N. Pont, V. Salvadó, C. Fontàs, *J. Membr. Sci.* 318 (1–2) (2008) 340–345.
- [11] B. Gupta, A. Deep, P. Malik, *Hydrometallurgy* 61 (2001) 65–71.
- [12] M. Benamor, Z. Bouariche, T. Belaid, M.T. Draa, *Sep. Purif. Technol.* 59 (2008) 74–84.
- [13] M.P. Gonzalez, I. Saucedo, R. Navarro, M. Avila, E. Guibal, *Ind. Eng. Chem. Res.* 40 (2001) 6004–6013.
- [14] L. Hinojosa Reyes, I. Saucedo Medina, R. Navarro Mendoza, J. Revilla Vazquez, M. Avila Rodriguez, E. Guibal, *Ind. Eng. Chem. Res.* 40 (2001) 1422–1433.
- [15] Q. Jia, Z.H. Wang, D.Q. Li, C.J. Niu, *Sep. Sci. Technol.* 38 (2003) 2025–2037.
- [16] N. Kabay, M. Demircioglu, H. Ekinci, M. Yuksel, M. Saglam, M. Streat, *React. Funct. Polym.* 38 (1998) 219–226.
- [17] N. Kabay, N. Gizli, M. Demircioglu, M. Yuksel, M. Saglam, M. Arda, U. Yuksel, B. Saha, M. Streat, *Chem. Eng. Commun.* 190 (2003) 936–947.
- [18] R. Navarro, I. Saucedo, A. Nunez, M. Avila, E. Guibal, *React. Funct. Polym.* 68 (2008) 557–571.
- [19] Y. Wang, C.Y. Wang, A. Warshawsky, B. Berkowitz, *Sep. Sci. Technol.* 38 (2003) 149–163.
- [20] J.L. Cortina, R. Arad-Yellin, N. Miralles, A.M. Sastre, A. Warshawsky, *React. Funct. Polym.* 38 (1998) 269–278.
- [21] J.L. Cortina, N. Miralles, *Solvent Extr. Ion Exch.* 15 (1997) 1067–1083.
- [22] J.L. Cortina, N. Miralles, A.M. Sastre, M. Aguilar, *React. Funct. Polym.* 32 (1997) 221–229.
- [23] J.L. Cortina, N. Miralles, M. Aguilar, A.M. Sastre, *Hydrometallurgy* 40 (1996) 195–206.
- [24] J.L. Cortina, N. Miralles, M. Aguilar, A. Warshawsky, *React. Funct. Polym.* 27 (1995) 61–73.
- [25] A.N. Pustam, S.D. Alexandratos, *React. Funct. Polym.* 70 (2010) 545–554.
- [26] R.A. Beauvais, S.D. Alexandratos, *React. Funct. Polym.* 36 (1998) 113–123.
- [27] D. Muraviev, M. Oleinikova, M. Valiente, *Langmuir* 13 (1997) 4915–4922.
- [28] N. Kabay, J.L. Cortina, A. Trochimczuk, M. Streat, *React. Funct. Polym.* 70 (2010) 484–496.
- [29] E. Guibal, T. Vincent, C. Jouannin, *J. Mater. Chem.* 19 (2009) 8515–8527.
- [30] E. Guibal, T. Vincent, *Sep. Sci. Technol.* 41 (11) (2006) 2533–2553.
- [31] T. Vincent, E. Guibal, R. Chiarizia, *Sep. Sci. Technol.* 42 (2007) 3517–3536.
- [32] V. Gallardo, R. Navarro, I. Saucedo, M. Avila, E. Guibal, *Sep. Sci. Technol.* 43 (2008) 2434–2459.
- [33] R. Navarro, I. Saucedo, M.A. Lira, E. Guibal, *Sep. Sci. Technol.* 45 (2010) 1950–1962.
- [34] K. Campos, R. Domingo, T. Vincent, M. Ruiz, A.M. Sastre, E. Guibal, *Water Res.* 42 (2008) 4019–4031.
- [35] K. Campos, T. Vincent, P. Bunio, A. Trochimczuk, E. Guibal, *Solvent Extr. Ion Exch.* 26 (2008) 570–601.
- [36] E. Guibal, K.C. Gavalan, P. Bunio, T. Vincent, A. Trochimczuk, *Sep. Sci. Technol.* 43 (2008) 2406–2433.
- [37] T. Vincent, A. Parodi, E. Guibal, *Sep. Purif. Technol.* 62 (2008) 470–479.
- [38] T. Vincent, A. Parodi, E. Guibal, *React. Funct. Polym.* 68 (2008) 1159–1169.
- [39] E. Guibal, A. Figuerola Piñol, M. Ruiz, T. Vincent, C. Jouannin, A.M. Sastre, *Sep. Sci. Technol.* 45 (2010) 1935–1949.
- [40] A. Cieszyńska, M. Regel-Rosocka, M. Wisniewski, *Pol. J. Chem. Technol.* 9 (2007) 99–101.
- [41] M. Regel-Rosocka, *Sep. Purif. Technol.* 66 (2009) 19–24.
- [42] A. Cieszyńska, M. Wisniewski, *Sep. Purif. Technol.* 73 (2010) 202–207.
- [43] M. Blahušák, Š. Schlosser, J. Marták, *React. Funct. Polym.* 71 (2011) 736–744.
- [44] J. Marták, Š. Schlosser, *Sep. Purif. Technol.* 57 (2007) 483–494.
- [45] C. van den Berg, N. Wierckx, J. Vente, P. Bussmann, J. de Bont, L. van der Wielen, *Biotechnol. Bioeng.* 100 (2008) 466–472.
- [46] R.-S. Juang, *Proc. Natl. Sci. Coun. ROC (A)* 23 (1999) 353–364.
- [47] S. Brunauer, P.H. Emmett, E. Teller, *J. Am. Chem. Soc.* 60 (1938) 309–319.
- [48] P.J. Branton, P.G. Hall, K.S. Sing, *J. Chem. Soc., Chem. Commun.* 16 (1993) 1257–1258.
- [49] H. Koshima, *Anal. Sci.* 2 (1986) 255–260.
- [50] I. Villaescusa, V. Salvado, J. de Pablo, M. Valiente, M. Aguilar, *React. Polym.* 17 (1992) 69–73.
- [51] M. Laatikainen, A. Paatero, *Hydrometallurgy* 79 (2005) 154–171.
- [52] R. Navarro, V. Gallardo, I. Saucedo, E. Guibal, *Hydrometallurgy* 98 (2009) 257–266.
- [53] B. Saha, R.J. Gill, D.G. Bailey, N. Kabay, M. Arda, *React. Funct. Polym.* 60 (2004) 223–244.
- [54] C.S. Brooks, *Metal Recovery from Industrial Wastes*, Lewis Publishers, Chelsea, MI, 1991, p. 215.
- [55] I. Puigdomenech, *Make Equilibrium Diagrams Using Sophisticated Algorithms (MEDUSA)*, vol. 3.1, Royal Institute of Technology, Stockholm, Sweden, 2002. <<http://www.kemi.kth.se/medusa>>.
- [56] M. Streat, *React. Polym.* 2 (1984) 79–91.
- [57] F. Helfferich, *Ion Exchange*, second ed., Dover Publications, Inc., Mineola, NY, 1995.
- [58] R.-S. Juang, C.-Y. Ju, *Ind. Eng. Chem. Res.* 37 (1998) 3463–3469.
- [59] R.-S. Juang, H.-C. Lin, *J. Chem. Technol. Biotechnol.* 62 (1995) 132–140.
- [60] R.-S. Juang, H.-C. Lin, *J. Chem. Technol. Biotechnol.* 62 (1995) 141–147.
- [61] J. Crank, *The Mathematics of Diffusion*, second ed., Oxford University Press, Oxford, UK, 1975, p. 414.
- [62] N. Nestle, R. Kimmich, *J. Phys. Chem.* 100 (1996) 12569–12573.
- [63] R. Navarro, I. Saucedo, M. Avila, M.P. Gonzalez, S. Garcia, E. Guibal, *Solvent Extr. Ion Exch.* 25 (2007) 273–297.